Proceedings of the ASME 2012 Conference on Smart Materials, Adaptive Structures and Intelligent Systems
SMASIS2012
September 19-21, 2012, Stone Mountain, Georgia, USA

SMASIS2012-8109

LOAD MONITORING OF AEROSPACE STRUCTURES USING MICRO-ELECTRO-MECHANICAL SYSTEMS (MEMS)

M. Martinez; B. Rocha; M. Li; G. Shi; A. Beltempo; R. Rutledge; M. Yanishevsky

National Research Council Canada, 1200 Montreal Road, Ottawa, ON, K1A-0R6, Canada
Phone: (613) 991-5360, Email: Marcias.Martinez@nrc-cnrc.gc.ca

ABSTRACT

The National Research Council of Canada has developed Structural Health Monitoring (SHM) test platforms for load and damage monitoring, sensor system testing and validation. One of the SHM platform consists of two 2.25 meter long, simple cantilever aluminium beams that provide a perfect scenario for evaluating the capability of a load monitoring system to measure bending, torsion and shear loads. In addition to static and quasi-static loading procedures, these structures can be fatigue loaded using a realistic aircraft usage spectrum while SHM and load monitoring systems are assessed for their performance and accuracy. In this study, Micro-Electro-Mechanical Systems (MEMS), consisting of triads of gyroscopes, accelerometers and magnetometers, were used to compute changes in angles at discrete stations along the structure. A Least Squares based algorithm was developed for polynomial fitting of the different data obtained from the MEMS installed in several spatial locations of the structure. The angles obtained from the MEMS sensors were fitted with a second, third and/or fourth order degree polynomial surface, enabling the calculation of displacements at every point. The use of a novel Kalman filter architecture was evaluated for an accurate angle and subsequent displacement estimation. The outputs of the newly developed algorithms were then compared to the displacements obtained from the Linear Variable Displacement Transducers (LVDT) connected to the structures. The determination of the best Least Squares based polynomial fit order enabled the application of derivative operators with enough accuracy to permit the calculation of strains along the structure. The calculated strain values were subsequently compared to the measurements obtained from reference strain gauges installed at different locations on the structure. This new approach for load monitoring was able to provide accurate estimates of applied strains and loads.

Keywords*: Micro-Electro-Mechanical Systems, Load Monitoring, Structural Health Monitoring, SHM, Health Usage Monitoring (HUMS), Holistic Structural Integrity Process (HOLSIP).*

INTRODUCTION

The National Research Council of Canada (NRC) has been participating in the development of a HOListic Structural Integrity Process (HOLSIP). This program is physics based and founded upon the primary idea that all failure mechanisms involved in the degradation of the structure are interconnected and should not be analyzed as merely the sum of individual mechanisms. In reality many failure mechanisms interact synergistically and are much more complex and challenging to understand, and thus the requirement for a holistic physics based analysis and design approach to structural integrity problems. The final goal of this holistic approach is to more accurately assess the reliability and structural integrity of aerospace structures [1,2,3]. However, many inputs are required for HOLSIP to provide the precise outputs that structural integrity engineers need to assess the remaining useful life of an aerospace structure relative to its original certification. In order to achieve this goal, NRC has been participating in the development of a road map that interconnects HOLSIP with other fields of research, as shown in Figure 1. This roadmap demonstrates how Usage Monitoring (UM) can be split into either Flight Condition Monitoring or Flight Load Monitoring. Flight Condition Monitoring refers to the use of machine learning algorithms and transfer functions to compute the load spectra applied to different structural components of the aircraft in flight. This process uses as input only the recorded flight state parameters obtained from a centralized set of sensors. The predicted load spectra can then be analyzed to identify and determine the fatigue degradation of critical components in the structure. Alternatively, the loads that the structure experiences during flight can be measured directly, rather than inferred from the flight state parameters. This second approach, referred to as Flight Load Monitoring, works well in combination with Structural Health Monitoring (SHM). Flight Load Monitoring can be achieved through the synthesis of flight load data, which

can be measured through the use of sensors installed in critical structural components. These loads, in combination with the initial condition of the structure, environmental spectra and material properties are introduced as inputs into HOLSIP (a physics based model) for determining useful remaining component life. This study concentrates on the direct measurement of critical component loads utilizing Micro-Electro-Mechanical System (MEMS).

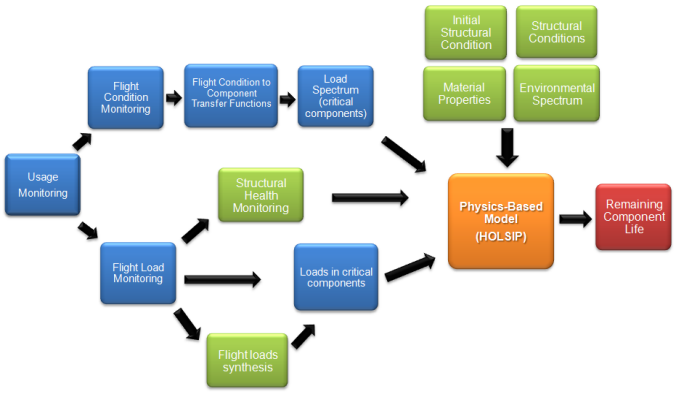

Figure 1: HOLSIP - Usage Monitoring Flow Chart.

The measurement of aircraft operation loads is an expensive task required for certification and for determining remaining useful component lives. Currently, during the development of a new aircraft, measured values of flight (manoeuvre / gust) and ground loads are required to check and validate the calculated design loads of the aircraft. In some cases, the design and fatigue loads used in original equipment full scale certification tests have been found to be substantially different from the way aircrafts are actually being used in service [4]. To overcome these shortfalls, to obtain a more efficient design of components (potentially with reduced weight) and increase aircraft safety, as well as provide vital information for aircraft operators and maintainers, continuous flight loads measurements and their comparison to static strength and fatigue flight envelope test data is required. Unfortunately, flight tests are typically of short duration and do not capture the long term fleet usage statistics and the entire envelope of static and fatigue load occurrences that are necessary for holistic structural evaluations. As mentioned, operational flight load measurements are currently accomplished by acquiring strain, flight parameters (pitch, roll, yaw, accelerations and rates, control surface deflections, air speed, angles of attack, etc), and "g" acceleration. Strain gauges are installed on critical aircraft structural components in flight tests and ground tests where known loads are applied at specific locations [5]. From the generated data and the known loading geometry, predictive loading equations are generated that are sufficient to calculate the bending moments, shear loads and torsion moments on the structure of interest. Complete validation of these loading equations requires the use of accelerometers to measure inertial loads, as well as the measurement of additional relevant flight parameters (such as altitude) for verification against the design flight regime "points in the sky" established during flight testing. In flight test aircraft, many strain gauges are utilized to generate the response equations. Since strain gauges drift and themselves undergo fatigue damage degradation, responses may become erroneous with time. The lack of reliability results in strain gauges not being widely applied on aircraft in service. As such, research on other sensor systems is justified.

The single use of accelerometers to measure loads is also well documented in the literature [6]. The three dimensional components of acceleration must be integrated twice to determine position, displacement and deformation, to enable the subsequent calculation of loads. When an integration of a mathematical equation is performed, an integration constant appears as part of the integration procedure that must be calculated through the application of a determined boundary condition. Furthermore, the execution of such integrations involves intrinsic numerical errors, augmented by the accumulation of errors included in the accelerometers' measurements (noise, biasing, etc) in the integration process. These errors have a significant impact on the integration results (velocities and displacements), as they are affected by the resolution, precision, and Signal to Noise Ratio (SNR) of the accelerometers.

Historically, accelerometers were installed near the centre of gravity on all Royal Air Force (RAF) aircraft in order to conduct fatigue life calculations for the airframes [7]. The Royal Canadian Air Force (RCAF) also followed this methodology and also developed computer algorithms which separated the effects of maneuvers and gusts [8]. Despite this instrumentation and besides the integration errors mentioned before, often there was still insufficient information to obtain complete load distributions on wings and tails. Unforeseen loading conditions, inherent structural degradations, or events that occur remotely from the location being monitored were not being captured by the sensors and were thus inadequately accounted for, making it impossible to perform structural evaluations without assumptions. Thus, to achieve detailed individual aircraft tracking, there is a requirement for an improved method of monitoring structural loads to facilitate obtaining load distributions directly.

MEMS are micro machines/mechanisms driven by, or generating electricity, capable of acting as actuators and sensors. With the rapid growth of consumer electronic technologies, the price of MEMS has dropped substantially and their application has widely increased to the extent that MEMS are now found in game consoles, inkjet printers, smart phones, and industrial and biomedical pressure sensors, to name a few [9,10]. In the application of MEMS as sensors, accelerometers, gyroscopes and magnetometers measuring three degrees of freedom, and temperature sensors have been incorporated in a single compact unit, for instance in the order of 40 mm by 40 mm by 15 mm. In this study, the use of MEMS for load monitoring through the distributed sensing of angular variation in an aircraft structure deformed by loading is

proposed and investigated. It is the objective of this study to demonstrate that distributed deformation, strain and subsequent load functions can be calculated using the angular data obtained from the MEMS sensors installed at different locations. The initial efforts in this study, with the mentioned objectives, and the initial experiments performed in a simple structural test rig are described.

METHODOLOGY AND SETUP

The approach utilized in the initial experiments performed as part of this study focuses on using MEMS sensors; located along the length of a cantilever beam that is part of the SHM Platform 1a. The principle focus of the methodology consists in determining structural deformation by measuring changes in angles at every MEMS sensor location. In this initial study, bending loading configurations were implemented, with different load values being quasi-statically applied. The final goal is to use a polynomial fitting to obtain a continuous deformation curve from the discrete MEMS sensors data, from which the applied loads can be computed.

NRC has acquired a total of five MEMS from GLI Interactive LLC. These MEMS were selected due to their compact size and their ability to provide data from imbedded accelerometers, gyroscopes, magnetometers and temperature sensors. Five of these MEMS were strategically located along the length of the beam in the use SHM Platform 1-A (Figure 2), in order to obtain angle changes at each station during beam deflection in real time. Besides raw and filtered sensor data, the MEMS are capable of outputting Euler angles and an orientation quaternion (global and local quaternion components) at frequencies as high as 100 Hz. Quaternions were first introduced by Sir William Rowan Hamilton in 1843. A detailed introduction to quaternion math can be found in [11]. For completeness, a basic overview of quaternion operations used in this study is provided below.

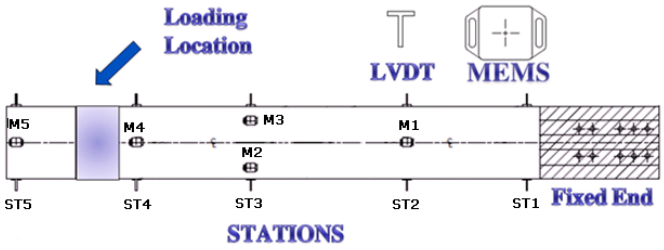

Figure 2: SHM Platform 1-A – MEMS and LVDTs Stations

Quaternion Math

A quaternion can be defined as a hyper complex number of rank four that relates two vectors in R^3 space. The rotation quaternions produced by the MEMS are quaternions of norm one. The quaternion q_1 expresses the relationship of the MEMS in its orientation at time t_1, represented by the orientation of a reference vector $\vec{v}_1$ with respect to the MEMS local coordinate reference system, and a fixed, unknown vector $\vec{v}_0$ which is part of R^3, as expressed in Figure 3 (a) and equation 1.

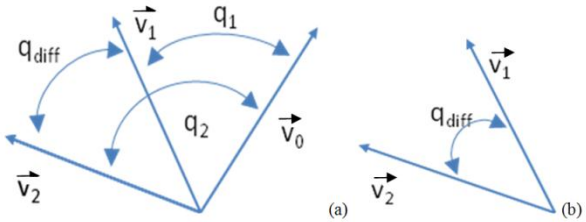

Figure 3: (a) Relationship between Vectors and Quaternions, (b) Relationship between Vectors $\vec{v}_2$ and $\vec{v}_1$ through Quaternion qdiff.

It is important to note that equation 1 makes use of the special triple multiplication of quaternion products:

$$\vec{v}_1 = q_1 \vec{v}_0 q_1^{-1} \quad (1)$$

Similarly, the quaternion q_2 produced by the MEMS provides, at time t_2, the transformation between $\vec{v}_2$ and vector $\vec{v}_0$, as shown in Figure 3 (a). Again this relationship between $\vec{v}_2$ and $\vec{v}_0$, can be expressed mathematically, as shown in equation 2:

$$\vec{v}_2 = q_2 \vec{v}_0 q_2^{-1} \quad (2)$$

However, since vector $\vec{v}_0$ is an unknown, the main interest is focused on determining the quaternion that transforms $\vec{v}_2$ to $\vec{v}_1$, which will be referred as q_{diff}, as shown in Figure 3(b). Similarly, vector $\vec{v}_2$ is related to $\vec{v}_1$, as shown in equation 4, using the transformation quaternion q_{diff}:

$$\vec{v}_2 = q_{diff} \vec{v}_1 q_{diff}^{-1} \quad (3)$$

The transformation quaternion q_{diff} in equation 3 can be resolved by substituting equation 1 into equation 3, as seen below:

$$\vec{v}_2 = q_{diff} q_1 \vec{v}_0 q_1^{-1} q_{diff}^{-1} \quad (4)$$

Comparing equation 4 to equation 2 and using the versor principle of addition of arcs, it is possible to find that the quaternion q_2, at time t_2, is related to the transformation quaternion q_{diff} and quaternion q_1, as shown in equation 5.

$$q_2 = q_{diff} q_1 \quad (5)$$

Thus, solving for the transformation quaternion q_{diff}, one finds that:

$$q_{diff} = q_2 q_1^{-1} \quad (6)$$

Equation 7 provides a very useful relationship, because it enables the evaluation of the change in angle from any time t_1

to t_2, without requiring the knowledge of the vector $\vec{v}_0$. This multiplication of two quaternions of norm one corresponds to the concatenation of angles in a sphere of radius one in R^4 [11]. Finally, the change in orientation can be computed from the definition that the transformation quaternion q_{diff} is related to the unit vector $\vec{r}_0$, corresponding to the axis of rotation, and the angle of rotation θ, as shown in the equations below for the scalar and vector components of the quaternion [12]:

$$q_{diff} = q_{diff_0} + \vec{q}_{diff} = \cos\left(\frac{\theta}{2}\right) + \vec{r}_0 \sin\left(\frac{\theta}{2}\right) \tag{7}$$

It is important to note that from equation 8, one can compute the rotation angle, as shown in equation 8:

$$\theta = 2\cos^{-1}(q_{diff_0}) \tag{8}$$

According to [11], the Euler angles γ, θ, ϕ, respectively yaw/heading, pitch/attitude/elevation and roll/bank, around z (vertical axis), y (transverse axis) and x (longitudinal axis) can be obtained from the transformation quaternion q_{diff} as:

$$\begin{aligned} \tan(\gamma) &= \frac{m_{12}}{m_{11}} \\ \sin(\theta) &= -m_{13} \\ \tan(\phi) &= \frac{m_{23}}{m_{33}} \end{aligned} \tag{9}$$

Where:

$$\begin{aligned} m_{11} &= 2 \cdot {q_{diff_0}}^2 + 2 \cdot {q_{diff_1}}^2 - 1 \\ m_{12} &= 2 \cdot q_{diff_1} \cdot q_{diff_2} + 2 \cdot q_{diff_0} q_{diff_3} \\ m_{13} &= 2 \cdot q_{diff_1} \cdot q_{diff_3} - 2 \cdot q_{diff_0} q_{diff_2} \\ m_{23} &= 2 \cdot q_{diff_2} \cdot q_{diff_3} + 2 \cdot q_{diff_0} q_{diff_1} \\ m_{33} &= 2 \cdot {q_{diff_0}}^2 + 2 \cdot {q_{diff_3}}^2 - 1 \end{aligned} \tag{10}$$

RESULTS

In our experiment, the LVDTs, whose locations are shown in Figure 2, provided the baseline data of the overall vertical displacement of the beam with respect to its reference or un-deformed state. This data was also used to compute the angles of the deformed shapes, along the beam's length. Since the form of the Euler-Bernoulli equation for the deflection of a cantilever beam with an applied point load yields a third order degree polynomial as the solution of the deformation field, a polynomial of the same order was fit tested to the discrete displacement data obtained from the LVDTs. As the data derived from the MEMS consists of beam slopes, the derivative of the third degree polynomial curve (fit to the LVDT data) was calculated to provide the baseline angular data to which the MEMS data can be compared. In Figure 4, the computed angles (slopes) from the MEMS at Station 5 are shown, for different values of applied bending loads (represented by the plateaus in the presented data). In this figure, several trends are shown and verified with respect to the derivative of the cubic polynomial constructed from the LVDT data, indicated by the circular dots in the figure, corresponding to the data labeled "Cubic Approximation". The data from each MEMS, in terms of slope, obtained from the Kalman filter provided by the MEMSs' manufacturer is also shown. The initial results lead us to consider the development of a custom Kalman filter for this application, whose improved performance is shown by the solid line denoting the values obtained using the NRC Kalman filter in Figure 4.

The NRC developed custom filter (based upon the Extended Kalman-Bucy filter architecture) [13], was found to accurately monitor changes in angles particularly well for the quasi-static scenario. It is foreseeable that as more dynamic load scenarios are tested, the NRC developed custom filter will need some fine adjustments to provide better estimates.

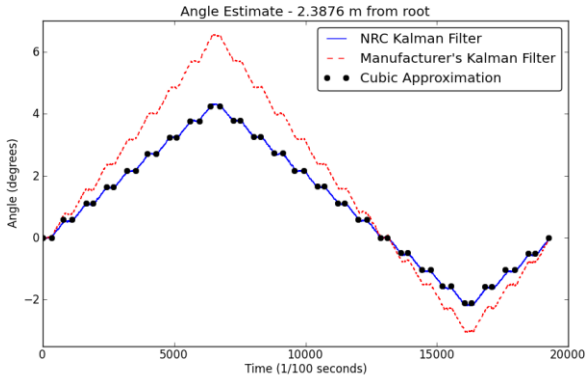

Figure 4: Computed Angles from MEMS at Station 5

The main drawback of this analytical method is that it requires a closed form solution for the structure in question. Although this is an efficient approach in the current case, it can be very challenging to obtain, particularly in the case of a complex structure, such as a fighter aircraft wing. For a more complex structure and/or loading condition, if an analytical solution is to be pursued, it is envisioned the need to divide the structural and loading domains in piecewise elements that can be simulated by a simpler structure, or loading condition.

Strain and Shear Forces

The strains and shear forces in the rectangular constant cross-section aluminum beam subjected to bending were estimated using the MEMS slope data. To arrive at these estimates, the MEMS readings were first post processed using the NRC developed custom filter (based upon the Extended Kalman-Bucy architecture), and then curve-fitted over the length/span of the beam. This fitting slope curve was then differentiated

using the Euler-Bernoulli beam theory differential equation, with the first derivative (of the rotation/slope given by the MEMS) yielding strain/moment distributions, and the second derivative yielding shear distribution. Under the appropriate boundary conditions, this inverse problem is well characterized and the fitted slope curve derivative should correspond to a forcing function matching the experimental load distribution. However, in practice it was found that the resulting load estimates were strongly affected by the behaviour of the fitting method. For example, a cubic spline interpolant was fitted, introducing inflections between data points, and thereupon causing each successive derivative (i.e. strains and shear force distributions) to fluctuate, when in reality they should have been smooth. It was found that the use of a piecewise least-squares fitting polynomial avoided these issues and yielded excellent results compared to strain gauge measurements and theoretical predictions. The optimal order of this polynomial fit was determined using a statistical test known as ANalysis Of VAriance (ANOVA), as explained in the next section. The optimum polynomial order predicted by ANOVA was found to agree with the order predicted by the Euler-Bernoulli beam theory.

Constrained Piecewise Least Square Fit

Rather than modeling the slope of the beam as a single continuous function, a piecewise function, split between two domains, was considered. One section of this piecewise function encompassed the region between the root of the beam (fully constrained) and the load applicator location, while the other covered the remaining span from the load applicator location to the tip of the beam. In both sections, a least squares fitting polynomial was calculated from the corresponding MEMS data, to estimate the slope distribution over the entire beam length. Two constraints that reflected the state of the physical system were imposed to relate these two curve fitting problems at their common boundary in their application domains. The first constraint ensured that the overall obtained fitted slope curve was continuous along the entire beam, by forcing each piecewise fit to hold the same value where they intersected (continuity). Similarly, the second constraint guaranteed continuity in the estimated moment distribution by enforcing the same condition to each piecewise derivative. In addition, two boundary conditions befitting a cantilever beam were imposed to enable the inverse Euler-Bernoulli problem to be solved. These boundary conditions constrained the beam to have zero slope at the root, and zero curvature at the free end.

In Figure 5, the dotted vertical line illustrates the boundary between domains (a.k.a. the location of the load applicator), while the points represent the data recorded by the MEMS. To increase the solution space, the number of MEMS was artificially augmented, as indicated by the triangular points in Figure 5.

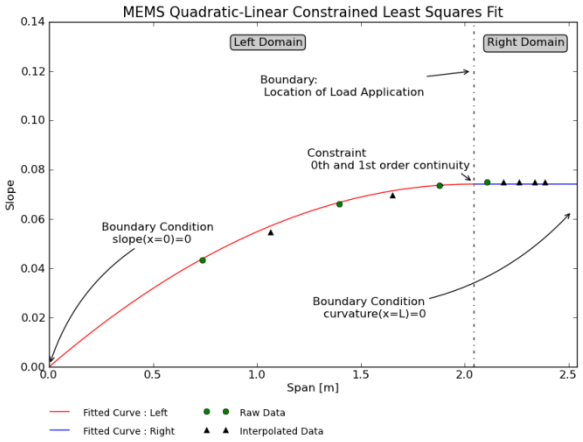

Figure 5: Slope versus Span of a Cantilever Beam for an applied static bending load

The additional points were required in order to have enough data points to test higher order polynomial approximations, enabling the assessment of the reliability of the ANOVA statistical test to determine the correct order of the polynomial fit. The additional points in the left domain region were obtained by linearly interpolating the data obtained from the two MEMS. In the second region, the augmented triangular points were artificially added to have the same slope (zero slope) as the one given by the MEMS sensor in that region, as shown in Figure 5.

As mentioned previously, an important task in the MEMS data fitting problem was to identify a suitable polynomial order of the fit for each segment. The use of the coefficient of determination (R^2) for that objective proved to be an inadequate, method, as it favored higher ordered polynomials, when in practice lower order models were more accurate. Typically, in unconstrained polynomial regression, the order would be determined using two ANOVA statistical tests [14]. The first ANOVA test would evaluate whether or not the particular polynomial fit appropriately captured the variance of the test data. If this criterion is met, then a second test would be needed to determine whether increasing the polynomial order significantly captures more of the data's variance. It is insufficient to simply rely on the first test, since once it is passed, any polynomial with a higher degree would be guaranteed to pass. Gallant and Fuller in [15] propose a similar method, using a ANOVA test for their segmented first order continuous, but unconstrained, polynomial model. Utilizing a similar approach and understanding that the ANOVA test was originally designed for unconstrained regression, this test was applied to each region of the MEMS data.

It was found that the developed testing method was sufficient to identify the order of the segmented polynomial. The results demonstrated that the MEMS data would be best represented by a quadratic-linear model, which is in accordance with the

theoretical results of the slope of a beam subject to a point load using the Euler-Bernoulli beam theory. Unlike unconstrained regression, the higher order models did not pass this test, a phenomenon likely owing to the influence of the imposed problem constraints. In Figure 6 (a), the resulting strain curve computed from the MEMS data is presented, for the same applied bending load as in Figure 5. For comparison, the data obtained from the strain gauges installed in the specimen is also presented. The corresponding shear force obtained from the MEMS data and the calculated shear force distribution and the load applicator from the data acquisition system are shown in Figure 6 (b).

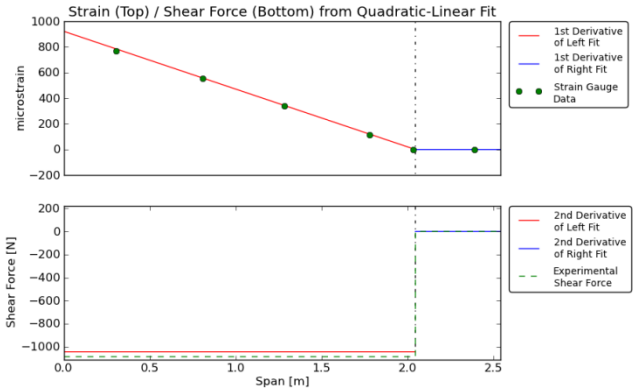

Figure 6: (a) Strain versus Span of a Cantilever Beam – SHM Platform 1-A; (b): Shear Force versus Span of a Cantilever Beam – SHM Platform 1-A.

Mathematically, the procedure used to identify the polynomial order was performed by calculating the sum of the square of regression (SSR) and the sum of squares of deviation (SSD) for each segment in the domain, as shown in the following equations:

$$SSR = \sum_i \left(\hat{Y}_i - \bar{Y}\right)^2 \tag{11}$$

and

$$SSD = \sum_i \left(\hat{Y}_i - Y_i\right)^2 \tag{12}$$

Where, $\hat{Y}_i$ denotes the regression estimate at X_i; $\bar{Y}$ is the arithmetic mean of the observed data set; and Y_i are the individual observations.
Secondly, the ratio of the mean squares is calculated as follows:

$$\left(\frac{SSR}{SSR}\right)\left(\frac{N-M-1}{M}\right)^{-1} \tag{13}$$

Where, M is the polynomial order and N is the number of data points.

Finally, this ratio was compared to the F distribution with degrees of freedom M and $N-M-1$, with a confidence value of 95%. If the ratio is within the F statistic, then it could be claimed (with at least 95% confidence) that the polynomial order sufficiently represented the data.

DISCUSSION

The use of MEMS for load monitoring has shown to produce results that closely match those obtained from the baseline instrumentation in the experimental setup. Allocating the minimum number of MEMS to each region of the domain required prior knowledge of the application. The structure and loading problem should be divided into locations where discontinuities occur either in the loading condition: point loads, breaks, etc, or where the structure changes in rigidity: Young Modulus, geometry / cross section, etc, such as in the locations where structural reinforcements are applied. Clearly, these discontinuities would subsequently affect the order of the applied best-fit polynomial. In the case of the NRC SHM Platform 1-A, the division between sections was intentionally placed coincident with the load applicator position, as the load applicator induced a step function discontinuity in the shear force. Since the constraints to the fit only required continuity in slope and moment, the second derivative (shear) of the fit was free to also be discontinuous at the same location. If instead a single continuous function spanning the entire length of the beam was pursued for modeling, it would inevitably encounter difficulties capturing the shear behaviour, since a smooth function could never truly approximate a step function. In practice, locating these discontinuities in shear on a real fighter aircraft wing (and thus the divisions, or domains) would be a matter of identifying the location of the pylons, to which missiles, external pods, cargo and engines attach; location of the beginning and end of fuel tanks, or aerodynamic elements, such as flaps, ailerons, etc, or even structural components, reinforcements and wing breaks. Should one or more boundaries arise in a more complex structure, such as a fighter aircraft wing and assuming that an analytical approach is considered, the number of divisions and the number of MEMS to use could easily be reformulated as a constrained least squares fit over M piecewise domains, with similar constraints for slope and curvature continuity enforced over each boundary.

CONCLUSIONS

The use of MEMS for load monitoring as an inverse problem has been proposed. The results demonstrate that it is feasible to accurately estimate strain and shear forces on a simple structure and for a simple loading condition. However, it is important to note that this was just the first step and that the problem of load estimation on more complex structures and for more complex loading conditions will have to be tackled carefully and using a knowledgeable approach, if an analytical method as presented in this paper is to be used.

An important observation in this methodology was the need to make a series of underlying assumptions, which included the prior knowledge of the point load application location, in order

to divide the structure into corresponding domains, with continuous boundary conditions having to be imposed at the interface of those domains. Although, this might seem as a large downside, it is important to note that in the case of a complex structure, this is still possible and might still be necessary in order to take advantage of the simplicity of utilizing an analytical approach. In the case where this is not achievable, the deformation of the structure could be obtained without any prior knowledge of the load application point through the use of Finite Element Method (FEM). This methodology might be very practical for complex case scenarios. In fact, based on the results obtained on the first SHM platform, further studies are being conducted on the second, more complex SHM platform, consisting of two 2.25 meter long representative aircraft aluminum stiffened skins, with riveted aluminum stringers. Due to the added complexities associated with this second structure, the computed displacements from the MEMS data are being applied as displacement boundary conditions on a detailed FEM of the structure, from which strain values are being calculated and compared to the experimental strain gauges.

Finally, the use of the NRC developed custom filter, based upon the extended Kalman-Bucy architecture, gave results that demonstrated how the use of mathematical predictive algorithms might aid in the acquisition of better measurements where the level of uncertainty is high. This type of approach could be combined with machine learning technologies to estimate loads through an optimization problem from which different kinds of computational tools could be used to estimate the most likely loading condition for a specific deformation function.

ACKNOWLEDGMENTS

This study was funded by the National Research Council Canada in collaboration with Defence Research Development Canada. Special thanks to Dr. Julio Valdés from the Institute for Information Technology at NRC, for his technical support on the statistical aspects of study.

REFERENCES

[1] http://www.holsip.com/, last accessed September 2011.

[2] Hoeppner, D. W., 2011, “Fretting fatigue considerations in holistic structural integrity based design processes (HOLSIP) – A continuing evolution”, Tribology International, Vol. 44, pp. 1364-1370.

[3] Liao, M. and Renaud, M., 2010, “Fatigue analysis for CF-18 component: wing fold shear-tie lug”, Procedia Engineering, Vol. 2(1), pp. 1673-1682, ISSN 1877-7058, 10.1016/j.proeng.2010.03.180.

[4] Simpson, D. L., Hiscocks, R. J. and Zavitz, D. – Canadair -, 1991, "A Parametric Approach to Spectrum Development", AGARD Conf. Proc. on Fatigue Management, AGARD-CP-506, December.

[5] Skopinski, T. H., Huston, W. B. and Aiken Jr., W. S., 1952, “Calibration of strain gauge installation in aircraft structures for the measurement of flight loads”, N.A.C.A. Report 1178, August.

[6] Engineeing Sciences Data Unit: “Estimation of the endurance of civil aircraft wing structures.” IHS Eng. Sciences Data Unit, Data Items #79024, October 1979.

[7] “Design and Airworthiness Requirements for Service Aircraft”, DEF STAN 00-970 Part 1/5, Section 3, P.23, Issue 5.

[8] Rugienius, A. V., 1977, “The Dissection of an Aircraft Loads Spectrum Produced by Peak-Counting Accelerometers”, LTR-ST-951, NAE, November.

[9] He, L., Zhang, J. and Jia, K., 2010, “Design and research of piezoelectric pump with MEMS flow sensor”, IEEE Conf. of Mechatronics and Automation (ICM), pp. 412-415.

[10] Pereyma, M., Motyka, I. and Lobur, M., 2007, “Perspectives of Smart RFID Tags Usage Fabricated by MEMS Technologies”, IEEE Perspective Technologies and Methods in MEMS Designs, pp. 113.

[11] Kuipers, J. B., 1999, *Quaternions and Rotation Sequences*, Princeton University Press, ISBN: 0-691-05872-5.

[12] Crassidis, J. L. and Markley, F. L., 1996, “Attitude Estimation Using Modified Rodrigues Parameters”, Flight Mechanics/Estimation Theory Symposium.

[13] Martinez, M., Rocha, B., Li, M., Beltempo, A., Yanishevsky, M., and Rutledge, R.S., 2011, "Micro-Electro-Mechanical Systems (MEMS) for Static and Quasi-Static Load Monitoring Applications", LTR-SMPL-2011-0222.

[14] Davis, J. C., 1986, *Statistics and Data Analysis in Geology*, 2nd Ed., John Wiley & Sons.

[15] Gallant, A. R. and Fuller, W. A., 1973, “Fitting segmented polynomial regression models whose join points have to be estimated”, J. Amer. Statist. Assoc., Vol. 68, pp. 144-147.